NB-IoT Physical Random Access Channels (NPRACHs) With Intercarrier Interference (ICI) Reduction

Jia-Chin Lin , *Senior Member, IEEE*

Abstract—This article proposes a novel technique to effectively detect superimposed preambles transmitted via narrowband Internet of Things (NB-IoT) physical random access channels (NPRACHs). Because the quasi-stationarity of these channels conserves local phase coherence over a few symbols, a symbol-level matched filter (SLMF) is used to effectively reduce out-band noise and interference without excessively accumulating phase increments occurring with the cross-correlation operations. The squared norms of the SLMF outputs are accumulated to test for the presence of a user equipment (UE). The false alarm and miss probabilities in the presence of frequency selectivity, time selectivity, and different channel gains through which the preambles of multiple UEs propagate are rigorously derived. To reduce intercarrier interference (ICI), which is mainly caused by different carrier frequency offsets (CFOs), a forward error reduction method based on interference regeneration and cancellation (IRnC) is studied. The IRnC method effectively reduces the miss probability but is not able to reduce the false alarm probability because the ICI cannot be perfectly regenerated and completely canceled. In addition, a closed-loop CFO compensation method is proposed to effectively maintain low false alarm and miss probabilities by sending quantized normalized CFO (NCFO) estimates back to the corresponding UEs via random access response (RAR) and reducing the CFO accordingly at the transmission end. Computer simulations confirm the theoretical analyses and show that the proposed technique achieves low false alarm and miss probabilities.

Index Terms—Detection, false alarm, intercarrier interference (ICI), narrowband Internet of Things (NB-IoT), NB-IoT physical random access channel (NPRACH), random access (RA).

I. Introduction

THE NARROWBAND Internet of Things (NB-IoT) is an application paradigm newly specified in the 3rd Generation Partnership Project (3GPP) specifications to simultaneously support numerous user equipment (UE) devices operating in the massive machine-type communication (mMTC) scenario. Similar to how a UE in a mobile communication network initiates a random access (RA) procedure to request uplink resources, a UE in the NB-IoT scenario transmits its preambles through an NB-IoT physical RA channel (NPRACH) with an initial coverage enhancement level

that is determined based on the power measurement of the reference signal received at the UE. An NPRACH consists of consecutive subcarriers allocated for preamble transmission. The NPRACH receiver at the serving base station (BS) needs to resolve the received signal, which is a superposition of signals transmitted from multiple active UEs with different channel impairments; identify the active UEs; and estimate the channel parameters on individual uplinks.

A previous study [1] completely described the physical-layer specifications of the NB-IoT in detail. Another study [2] designed a hopping pattern to effectively estimate the Time of Arrival (ToA). Another prior study [3] proposed an optimization approach to jointly determine the medium access control (MAC) parameters so as to maximize the access success probability under a latency constraint. A pioneering study [4] proposed a receiving technique for NPRACH detection and ToA estimation. Lin et al. [4] intuitively evaluated the 2-D cross-correlation function via a 2-D discrete-time Fourier transform (DFT). Although several existing works in the NB-IoT research area have followed the intuitive method proposed in [4], called the 2-D fast Fourier transform (FFT), the 2-D cross-correlation function itself (called the ambiguity function in radar research) has also been commonly used [5], and a joint maximum-likelihood estimation (JMLE) technique has been theoretically derived in several previous studies [6], [7]. A previous study [8] explicitly studied the determination of an appropriate decision threshold for NPRACH preamble detection in NB-IoT systems. Although the title of [8] claims that the proposed threshold determination method attains optimality, the proposed decision threshold is actually chosen as an average between the maximum and minimum magnitudes of the DFT demodulator outputs; therefore, it can more correctly be considered intuitive and heuristic rather than optimal. Another study [9] analyzed the NPRACH detection probability and proposed a field programmable gate array (FPGA) receiver implementation. Nevertheless, the techniques studied in [4], [8], and [9] do not consider the received signal as a superposition of multiple uplink signals propagating through different frequency-selective fading channels with different carrier frequency offsets (CFOs) and different ToAs; therefore, they not only overly simplify the performance evaluation of the detection process but also disregard the intercarrier interference (ICI) effects resulting from different CFOs. However, such ICI unavoidably increases both the false alarm and miss probabilities.

A previous study [10] proposed an NPRACH method based on singular value decomposition (SVD) of the covariance matrix. The technique proposed in [10] relies on covariance analysis and therefore requires a large number of received preambles to enhance the accuracy of detection and estimation, especially in the low signal-to-noise ratio (SNR) regime [11]. Recently, Aoudia et al. [12] and Kumar and Balasubramanya et al. [13] studied deep learning methods to achieve NPRACH detection in NB-IoT systems. However, deep learning methods are inappropriate for handling initial synchronization because they usually require a high signal-to-interference-plus-noise ratio (SINR) and many training preambles while not considering various channel impairments, e.g., complex channel gains, CFOs, time errors (TEs), and ICI. Another recent study [14] addressed differential processing with minimum combining for NPRACH detection. However, differential processing suffers not only from noise enhancement under low-SNR conditions but also from 3-dB SNR degradation under high-SNR conditions [15]. More recently, Chougrani et al. [16], Liu and Gokhale [17], and Kodheli et al. [18] investigated RA procedures in nonterrestrial networks (NTNs), which exhibit considerably increased delays and relatively large CFOs. However, these studies [16], [17], [18] focused only on the problem of large differential delays under the assumption of no ICI. All of the aforementioned studies [4], [8], [9], [10], [12], [13], [14], [16], [17] lack any simulated or analytical results to demonstrate the false alarm probability. In fact, few, if any, previous works in the literature have considered the ICI effects resulting from multiple nonnegligible CFOs. As a result, no previous work has studied any technique for overcoming the associated challenges.

Notably, for NPRACHs, the signal received at a BS is composed of many single-tone frequency-hopping preambles, instead of the orthogonal frequency-division multiple access (OFDMA) signals used in 3GPP long-term evolution advanced (LTE-A) downlink transmissions or the single-carrier frequency-division multiple access (SC-FDMA) signals used in 3GPP LTE-A uplink transmissions. Unlike in OFDMA, the cyclic prefixes (CPs) used in NPRACHs cannot be exploited to maintain the orthogonality among subcarriers. Therefore, the DFT-based demodulation used in OFDMA systems (or the 2-D DFT-based demodulation proposed in [4]) is never needed. Unlike in SC-FDMA, no guard band is reserved between the neighboring frequency bands used for different UEs in NB-IoT systems. Therefore, multiple access interference (MAI) is unavoidably present when different CFOs occur in different UEs.

This article proposes an NPRACH detection technique to address a superimposed signal received via multiple uplinks with different CFOs, different TEs, and different time-varying frequency-selective fading channels. The decision threshold for the presence of an individual NPRACH preamble is theoretically derived in accordance with the Neyman–Pearson criterion [19, pp. 132–133] because the (log-)likelihood function in hypothesis 1 suffers from nuisance parameters, i.e., channel gains. Accordingly, the false alarm and miss probabilities obtained using the proposed

technique are derived via statistical analysis. An interference regeneration and cancellation (IRnC) method operating similarly to that in a previous study [20] is investigated to reduce the miss probability. In addition, a closed-loop CFO compensation (CLCC) mechanism is proposed. This mechanism sends quantized CFO estimates back to the corresponding UEs via RA response (RAR), i.e., Message 2 of the PRACH procedure [18]. Accordingly, CFO compensation can be performed at each UE, thus effectively reducing both the false alarm and miss probabilities by avoiding ICI effects. The remainder of this article is organized as follows. The signal modeling and problem formulation are described in Section II. Analytical results and simulation results are compared in Section III, and the IRnC and CLCC methods are also studied. Finally, concluding remarks are provided in Section IV.

II. SIGNAL MODELING AND PROBLEM FORMULATION

The discrete-time baseband equivalent signal transmitted from the uth UE can be written as follows:

$$s'_u[k] = \sqrt{P_s}\, e^{j2\pi v\left[u, \lfloor k\rfloor_{/N_{\mathrm{SG}}}\right]\left(\left|\lfloor k\rfloor_{/N_{\mathrm{SG}}} - N_{\mathrm{cp}}\right|_{/N}\right)} \tag{1}$$

where k is the time index, which represents the time instant kt_s, with $t_s = T/N$, T, and N representing the sampling period, the symbol duration, and the number of samples in a symbol, respectively; N_{cp} and N_{SG} represent the number of samples in a CP and the number of samples in a symbol group (SG), respectively; $P_s = E_s/t_s$ represents the sample power, with E_s representing the sample energy; $v[u, k]$ denotes the subcarrier frequency used in the kth SG from the uth UE; and $\lfloor\cdot\rfloor$ and $|\cdot|$ are the floor and modulo operators, respectively, i.e., $\lfloor x\rfloor_{/y}$ and $|x|_{/y}$ represent the integer part and remainder, respectively, of x/y. The superimposed signal received at the BS can be written as follows:

$$\begin{aligned} r[k] &= \frac{r'[k]}{\sqrt{P_s}} \\ &= \sum_{u=0}^{U-1} w_{u,v}\, s_u[k - l_u]\, e^{j\left(2\pi\frac{\epsilon_u(k - l_u)}{N} + \phi_0\right)} + n[k] \end{aligned}$$

$$k = 0, 1, 2, \ldots \tag{2}$$

where

$$r'[k] = \sum_{u=0}^{U-1} w_{u,v}\, s'_u[k - l_u]\, e^{j\left(2\pi\frac{\epsilon_u(k - l_u)}{N} + \phi_0\right)} + n'[k].$$

$s_u[k] = s'_u[k]/\sqrt{P_s}$; $n[k] = n'[k]/\sqrt{P_s}$; and $w_{u,v}$, ϵ_u, l_u and ϕ_0 represent the complex-valued channel gain at frequency v, the normalized CFO (NCFO), the TE occurring with the uth uplink and the initial phase error resulting from the front-end noncoherent downconversion process, respectively. The power normalization applied above, i.e., $1/\sqrt{P_s}$, is used only for simplicity of representation. The NCFO ϵ_u in (2) is the CFO normalized with respect to the subchannel bandwidth (also known as the subcarrier spacing) $\Delta f = 1/T$ as follows:

$$\epsilon_u = \frac{\varepsilon_u}{\Delta f}$$

where ε_u represents the uth CFO in hertz (Hz). $n'[k] = n'(kt_s)$ denotes the additive white Gaussian noise (AWGN) $n'(t)$ sampled at kt_s, whose power spectral density (PSD) is $S_n(f) = N_0$. Here, the receive filter has a null-to-null bandwidth of $1/t_s$, and therefore, the sampled noise $n'[k]$ is an uncorrelated Gaussian sequence with zero mean and a variance of $2\sigma_n^2 = N_0/t_s$. Because of the normalization relation $n[k] = n'[k]/\sqrt{P_s}$, $n[k]$ is an uncorrelated Gaussian sequence with zero mean and a variance of $2\bar{\sigma}_n^2 = 2\sigma_n^2/P_s = (E_s/N_0)^{-1}$. The qth output of a symbol-level matched filter (SLMF) when applied to the mth SG from the uth UE can be written as follows:

$$\xi_u(m, q) = \frac{1}{N} \cdot \sum_{k=mN_{SG}+qN+N_{cp}}^{mN_{SG}+qN+N_{cp}+(N-1)}$$
$$r[k]e^{-j2\pi\nu[u,m]\left(\left|\left.k\right|_{/N_{SG}}-N_{cp}\right|_{/N}\right)}$$
$$= C_u(m, q) + I_u(m, q) + n(m, q)$$
$$m = 0, 1, 2, 3; \quad q = 0, 1, 2, 3, 4 \qquad (3)$$

where

$$C_u(m, q) = w_{u,v}e^{j\phi_{u,1}}e^{j2\pi\epsilon_u \frac{mN_{SG}+qN+N_{cp}+N-1}{N}}\frac{\sin(\pi\epsilon_u)}{N\sin\left(\frac{\pi\epsilon_u}{N}\right)}$$

is the desired term, conveying the cross-correlation, $\phi_{u,1} = -2\pi(\nu[u, m] + \epsilon_u)l_u + \phi_{u,0}$

$$I_u(m, q) = \frac{1}{N} \sum_{k=mN_{SG}+qN+N_{cp}}^{mN_{SG}+qN+N_{cp}+(N-1)} \sum_{\substack{u'=0 \\ u'\neq u}}^{U-1} w_{u',v}$$
$$\times e^{\left(j2\pi\nu\left[u', \lfloor k-l_{u'}\rfloor_{/N_{SG}}\right](k-l_{u'})\right)}e^{j\left(2\pi\frac{\epsilon_{u'}(k-l_{u'})}{N}\right)}$$
$$\times e^{\left(-j2\pi\nu[u,m]\left(\left|\left.k\right|_{/N_{SG}}-N_{cp}\right|_{/N}\right)\right)}$$

is the ICI term, which predominantly results from the nonnegligible CFOs occurring in adjacent subchannels; and

$$n(m, q) = \frac{1}{N} \sum_{k=mN_{SG}+qN+N_{cp}}^{mN_{SG}+qN+N_{cp}+(N-1)} n[k]e^{-j2\pi\nu[u,m]\left(\left|\left.k\right|_{/N_{SG}}-N_{cp}\right|_{/N}\right)}$$

is the noise term, which is a complex-valued Gaussian random variable (RV) with zero mean and a variance of $2\sigma_N^2 = 2\bar{\sigma}_n^2/N = (E_{symb}/N_0)^{-1}$, with $E_{symb} = NE_s$ denoting the symbol energy.

A. NPRACH Detection

The detection process for testing whether the uth UE is sending NPRACH preambles can be converted into the following binary hypothesis testing problem. The detection metric over L preambles can be formulated as the accumulation of the squared envelopes of the SLMF outputs, i.e.,

$$X_{u,L} = \sum_{l=0}^{L-1} \zeta_u(l) \qquad (4)$$

where

$$\zeta_u(l) = \sum_{m=0}^{3} \sum_{q=0}^{4} |\xi_u(m, q)|^2.$$

Under hypothesis 1, denoted by H_1, which states that the uth UE is active, $X_{u,L}$ has a noncentral χ^2 distribution with $40L$ degrees of freedom (DOFs). Thus, the conditional probability density function (PDF) and conditional cumulative distribution function (CDF) of $X_{u,L}$ can be written as [21, p. 46]

$$f_{X_{u,L}}(x|H_1, \rho)$$
$$= \frac{1}{2\sigma_N^2}\left(\frac{x}{\rho^2}\right)^{10L-\frac{1}{2}}e^{-\frac{x+\rho^2}{2\sigma_N^2}}\ I_{20L-1}\left(\frac{\rho\sqrt{x}}{\sigma_N^2}\right) \quad x \geq 0 \quad (5)$$

and

$$F_{X_{u,L}}(x|H_1, \rho) = 1 - Q_{20L}\left(\sqrt{\frac{\rho^2}{\sigma_N^2}}, \sqrt{\frac{x}{\sigma_N^2}}\right), \ x \geq 0 \qquad (6)$$

respectively, where the undetermined parameter

$$\rho = \left(5\sum_{l=0}^{L-1}\sum_{m=0}^{3}|w_{u,v}|^2\right)^{\frac{1}{2}}$$

represents the noncentrality, in which $w_{u,v}$ remains unchanged within an SG because of the quasi-stationarity of the subchannels

$$I_\alpha(x) = \sum_{k=0}^{\infty}\frac{(x/2)^{\alpha+2k}}{k!\Gamma(\alpha + k + 1)}, \qquad x \geq 0$$

is the modified Bessel function of the first kind and order α

$$\Gamma(x) = \int_0^{\infty} t^{x-1}e^{-t}dt$$

is the gamma function; and

$$Q_m(a, b) = \int_b^{\infty} x\left(\frac{x}{a}\right)^{m-1}e^{-(x^2+a^2)/2}I_{m-1}(ax)\ dx$$

is the generalized Marcum Q-function [21, p. 47]. Notably, $w_{u,v}$ in ρ, as written below (6), depends on both m and l due to frequency and time selectivity, respectively.

Under hypothesis 0, denoted by H_0, which states that the uth UE is not present, $X_{u,L}$ has a central χ^2 distribution with $40L$ DOFs [21, p. 45]. The conditional PDF and conditional CDF of $X_{u,L}$ can be written as follows:

$$f_{X_{u,L}}(x|H_0) = \frac{1}{2^{20L}\Gamma(20L)\sigma_N^{40L}}x^{20L-1}e^{-\frac{x}{2\sigma_N^2}}, \ x \geq 0 \qquad (7)$$

and

$$F_{X_{u,L}}(x|H_0) = 1 - e^{-\frac{x}{2\sigma_N^2}}\sum_{k=0}^{20L-1}\frac{1}{k!}\left(\frac{x}{2\sigma_N^2}\right)^k, \ x \geq 0, \qquad (8)$$

respectively. In practice, the noncentrality ρ in (5) resulting from the channel gains cannot be obtained prior to NPRACH detection; therefore, it is regarded as a nuisance parameter in the NPRACH detection process. Because $f_{X_{u,L}}(x|H_1, \rho)$ in (5) contains this undetermined parameter, NPRACH preamble detection can only be conducted by applying the Neyman–Pearson criterion [19, pp. 132–133]. The false alarm probability of NPRACH preamble detection is usually required to be lower than the nominal false alarm probability (NFAP) α_{nml}. Given the NFAP provided in the specifications, e.g., $\alpha_{nml} =$

10^{-3}, the decision threshold T can be determined by solving the following equation:

$$\alpha_{\text{nml}} = \int_T^\infty f_{X_{u,L}}(x|H_0)\, dx = 1 - F_{X_{u,L}}(T|H_0)$$

$$= e^{-\frac{T}{2\sigma_N^2}} \sum_{k=0}^{20L-1} \frac{1}{k!}\left(\frac{T}{2\sigma_N^2}\right)^k. \tag{9}$$

Once the decision threshold T has been determined via numerical methods, the probability of successful detection can be written as follows:

$$P_D\left(\frac{E_{\text{symb}}}{N_0}\right)\bigg|\rho = 1 - F_{X_{u,L}}(T|H_1, \rho) = \mathsf{Q}_{20L}\left(\frac{\rho}{\sigma_N}, \frac{\sqrt{T}}{\sigma_N}\right)$$

$$= \mathsf{Q}_{20L}\left(\rho\sqrt{\frac{2E_{\text{symb}}}{N_0}}, \sqrt{T\frac{2E_{\text{symb}}}{N_0}}\right). \tag{10}$$

In accordance with the commonly used Clarke channel model, in which scatters are assumed to be uniformly distributed [22], the complex-valued channel gains $w_{u,v}$ are usually modeled as zero-mean complex Gaussian RVs with variance $2\sigma_w^2$ for a Rayleigh fading channel. Because $w_{u,v}$ remains unchanged for an SG, the expression given for ρ below (6) can be rewritten as follows:

$$\rho = \sqrt{5}\bar{\rho}$$

where $\bar{\rho} = \left(\sum_{l=0}^{L-1}\sum_{m=0}^3 |w_{u,v}|^2\right)^{1/2}$. Note that $\bar{\rho}$ has a Nakagami-m distribution with the following PDF [21, p. 49]:

$$p(\bar{\rho}) = \frac{\bar{\rho}^{8L-1}}{2^{4L-1}(\sigma_w^2)^{4L}\Gamma(4L)} e^{-\frac{\bar{\rho}^2}{2\sigma_w^2}}, \qquad \bar{\rho} \geq 0. \tag{11}$$

Therefore, the PDF of ρ can be written as follows:

$$p(\rho) = p(\bar{\rho})\left\|\frac{d\bar{\rho}}{d\rho}\right\|\bigg|_{\bar{\rho}=\frac{\rho}{\sqrt{5}}} = \frac{\frac{1}{\sqrt{5}}\left(\frac{\rho}{\sqrt{5}}\right)^{8L-1} e^{-\frac{\rho^2}{10\sigma_w^2}}}{2^{4L-1}(\sigma_w^2)^{4L}\Gamma(4L)}, \quad \rho \geq 0. \tag{12}$$

The average detection probability and the average miss probability can be written as follows:

$$\bar{P}_D\left(\frac{E_{\text{symb}}}{N_0}\right) = \int_0^\infty \left(P_D\left(\frac{E_{\text{symb}}}{N_0}\right)\bigg|\rho\right)p(\rho)\, d\rho \tag{13}$$

and

$$\bar{P}_M\left(\frac{E_{\text{symb}}}{N_0}\right) = 1 - \bar{P}_D\left(\frac{E_{\text{symb}}}{N_0}\right), \tag{14}$$

respectively.

B. Joint Estimation of the NCFO and TE

When the uth UE is considered active based on the NPRACH detection process described in the preceding section, the received signal expression given in (2) can be rewritten as follows:

$$r[k] = \sum_{u'=0}^{U-1} w_{u',v} s_{u'}[k - l_{u'}] e^{j\left(2\pi\frac{\epsilon_{u'}}{N}(k-l_{u'})+\phi_{u',0}\right)} + n[k]$$

$$= w_{u,v} s_u[k - l_u] e^{j\left(2\pi\frac{\epsilon_u}{N}(k-l_u)+\phi_{u,0}\right)} + n_\iota[k] \tag{15}$$

where the former term represents the preamble sent from the uth UE and is the desired term, and the latter term is given as follows:

$$n_\iota[k] = \iota[k] + n[k].$$

This expression in turn contains an ICI term, expressed as

$$\iota[k] = \sum_{\substack{u'=0 \\ u'\neq u}}^U w_{u',v} s_{u'}[k - l_u] e^{j\left(2\pi\frac{\epsilon_{u'}}{N}(k-l_{u'})+\phi_{u,0}\right)}$$

and an AWGN term $n[k]$ with zero mean and a variance of $2\bar{\sigma}_n^2$. The ICI term largely arises from adjacent channels and does not have an analytical model. The following analysis mainly focuses on the effects of the AWGN term.

When the channel gain $w_{u,v}$ and initial phase $\phi_{u,0}$ are regarded as nuisance parameters, the likelihood function and log-likelihood function of the NCFO ϵ_u and TE l_u of the uth uplink transmission can be written as follows:

$$\tilde{\mathsf{L}}\left(\begin{bmatrix}\epsilon_u \\ l_u\end{bmatrix}; w_{u,v}, \phi_{u,0}\right)$$

$$= \prod_{k=0}^{N-1} \frac{1}{2\pi\bar{\sigma}_n^2} e^{-\frac{\left(r[k]-w_{u,v}e^{j\left(2\pi\left(v+\frac{\epsilon_u}{N}\right)(k-l_u)+\phi_{u,0}\right)}\right)^2}{2\bar{\sigma}_n^2}}$$

$$= \left(2\pi\bar{\sigma}_n^2\right)^{-N}$$

$$\times \exp\left(-\frac{\sum_{k=0}^{N-1}\left(r[k]-w_{u,v}e^{j\left(2\pi\left(v+\frac{\epsilon_u}{N}\right)(k-l_u)+\phi_{u,0}\right)}\right)^2}{2\bar{\sigma}_n^2}\right) \tag{16}$$

and

$$\mathsf{L}\left(\begin{bmatrix}\epsilon_u \\ l_u\end{bmatrix}; w_{u,v}, \phi_{u,0}\right)$$

$$= -N\log\left(2\pi\bar{\sigma}_n^2\right) - \frac{1}{2\bar{\sigma}_n^2}\sum_{k=0}^{N-1}\left(r[k] - w_{u,v}\right.$$

$$\times \left.\exp\left(j\left(2\pi\left(v+\frac{\epsilon_u}{N}\right)(k-l_u)+\phi_{u,0}\right)\right)\right)^2 \tag{17}$$

respectively. As a result, the JMLE of ϵ_u and l_u with nuisance parameters $w_{u,v}$ and $\phi_{u,0}$ can be written, as shown in (18), at the bottom of the next page, in which

$$\kappa(\epsilon_u, l_u) = \sum_{k=0}^{N-1} r[k]\exp\left(-j\left(2\pi\left(v+\frac{\epsilon_u}{N}\right)(k-l_u)\right)\right)$$

represents the cross-correlation of the received signal and a replica of the transmitted signal with a frequency shift ϵ_u and a TE l_u, $\Re\{\cdot\}$ denotes the operation of taking the real part of the argument

$$\phi_W = \tan^{-1}\frac{\Im\{w_{u,v}\}}{\Re\{w_{u,v}\}}$$

$$\phi_M = \tan^{-1}\frac{\Im\left\{\sum_{k=0}^{N-1} r[k]\exp\left(-j\left(2\pi\left(v+\frac{\epsilon_u}{N}\right)(k-l_u)\right)\right)\right\}}{\Re\left\{\sum_{k=0}^{N-1} r[k]\exp\left(-j\left(2\pi\left(v+\frac{\epsilon_u}{N}\right)(k-l_u)\right)\right)\right\}}$$

and $\Im\{\cdot\}$ denotes the operation of taking the imaginary part of the argument. Note that the bottom line of (18) is reached

because $|w_{u,v}|$ and $\Re\{e^{-j(\phi_{u,0}+\phi_W-\phi_M)}\}$ are irrelevant to the JMLE of ϵ_u and l_u. The JMLE of ϵ_u and l_u in (18) is built as a bank of time-domain (TD) matched filters (TDMFs). The TDMF outputs can be written as follows:

$$\xi\left(\hat{\epsilon}_u, \hat{l}_u\right) = \frac{1}{N}\sum_{k=0}^{N-1} r[k] e^{-j\left(2\pi\left(v+\frac{\hat{\epsilon}_u}{N}\right)\left(k-\hat{l}_u\right)\right)}. \qquad (19)$$

By adopting the notations $\Delta\epsilon_u = \epsilon_u - \hat{\epsilon}_u$ and $\Delta l_u = l_u - \hat{l}_u$, (19) can be rewritten as follows:

$$\Psi(\Delta\epsilon_u, \Delta l_u) = w_{u,v}\psi(\Delta\epsilon_u, \Delta l_u) + N_\psi \qquad (20)$$

where

$$\psi(\Delta\epsilon_u, \Delta l_u) = \frac{\sin(\pi\Delta\epsilon_u)}{N\sin\left(\pi\frac{\Delta\epsilon_u}{N}\right)} e^{j\pi\frac{\Delta\epsilon_u}{N}(N-1-l_u)}$$

and

$$N_\psi = \frac{1}{N}\sum_{k=0}^{N-1} n_\iota[k] \exp\left(-j\left(2\pi\left(v+\frac{\hat{\epsilon}_u}{N}\right)\left(k-\hat{l}_u\right)\right)\right).$$

In the context of radar analysis, the magnitude of $\psi(\Delta\epsilon_u, \Delta l_u)$ is usually called the ambiguity function [5]. The ambiguity function is depicted in Fig. 1. The modified Cramér-Rao lower bounds (MCRLBs) can further be found in the form of [6, eq. (11)]. However, this article does not further derive any CR-like bounds because the theoretical benchmarks are not concise due to the lack of accurate ICI statistics in the literature. Hence, the performance degradation caused by the ICI term is instead addressed via Monte Carlo simulations.

III. SIMULATIONS

For rapid deployment and coexistence with 3GPP LTE-A networks, NB-IoT technology follows the 3GPP physical-layer specifications [1]. The system parameters applied for the NB-IoT have been well investigated in the previous study [1]. The parameter settings used here are briefly mentioned as follows. In the frequency domain, one LTE physical resource block (PRB) of 180 kHz is allocated for NB-IoT uplink transmission. The subcarrier spacing used is $\Delta f = 3.75$ kHz. Therefore, this 180-kHz NB-IoT band can accommodate 48 NB-IoT subchannels. In this article, the NB-IoT uplinks occupy the guard bands of an LTE band. Specifically, 24 subchannels are in the upper guard band, while the other 24 subchannels are in the lower guard band. Frequency-selective fading channels are
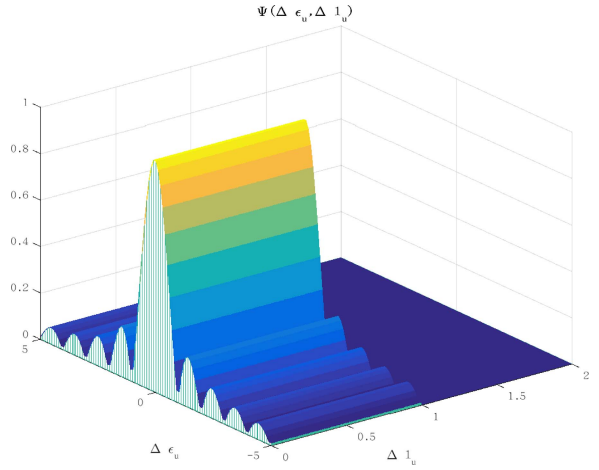

Fig. 1. Ambiguity function $|\psi(\Delta\epsilon_u, \Delta l_u)|$.

considered. The NPRACH preambles of different SGs from a single UE propagate through different subchannels, thus experiencing different subchannel gains.

In the time domain, an NPRACH preamble consists of four SGs. An SG consists of five symbols and one CP with a length of $T/4$. Therefore, the symbol duration and the CP length are $T = 1/\Delta f = 266.67~\mu s$ and $66.67~\mu s$, respectively. One symbol duration consists of $N = 512$ samples. This article considers time-varying and quasi-stationary channels. In other words, the subchannel gains remain unchanged within one SG duration, but they are updated every SG by drawing from the Jakes' fading channel model [23]. To reduce complexity, the received signal should be demultiplexed into the low-frequency band and then filtered by a first-order infinite-impulse-response (IIR) low-pass filter (LPF) with the following transfer function:

$$H(z) = \frac{1-a}{1-az^{-1}}, \quad a = \exp\left(-\frac{2\pi}{M_{dn}}\right). \qquad (21)$$

The output stream of the IIR LPF can be downsampled by M_{dn} times without loss of preamble information. Because the NPRACH preambles occupy at most 48 subchannels and the entire LTE bandwidth accommodates $N = 512$ subchannels, $M_{dn} = 8$ ($<512/48$) is chosen unless otherwise mentioned. To enhance the accuracy of CFO estimation, frequency-domain (FD) upsampling is conducted by dividing each subchannel into M_{up} levels. The FD upsampling can

$$\begin{aligned}\begin{bmatrix}\hat{\epsilon}_u \\ \hat{l}_u\end{bmatrix} &= \arg\max_{\epsilon_u, l_u} \mathsf{L}\left(\begin{bmatrix}\epsilon_u \\ l_u\end{bmatrix}; w_{u,v}, \phi_{u,0}\right) \\ &= \arg\max_{\epsilon_u, l_u}\left\{-\frac{1}{2\tilde{\sigma}_n^2}\sum_{k=0}^{N-1}\left(r[k] - w_{u,v}\exp\left(j\left(2\pi\left(v+\tfrac{\epsilon_u}{N}\right)(k-l_u)+\phi_{u,0}\right)\right)\right)^2\right\} \\ &= \arg\max_{\epsilon_u, l_u}\Re\left\{w_{u,v}^*\sum_{k=0}^{N-1} r[k]\exp\left(-j\left(2\pi\left(v+\tfrac{\epsilon_u}{N}\right)(k-l_u)+\phi_{u,0}\right)\right)\right\} \\ &= \arg\max_{\epsilon_u, l_u}|w_{u,v}|\left|\sum_{k=0}^{N-1} r[k]\exp\left(-j\left(2\pi\left(v+\tfrac{\epsilon_u}{N}\right)(k-l_u)\right)\right)\right|\Re\left\{e^{-j(\phi_{u,0}+\phi_w-\phi_M)}\right\} \\ &= \arg\max_{\epsilon_u, l_u}|\kappa(\epsilon_u, l_u)|\end{aligned} \qquad (18)$$
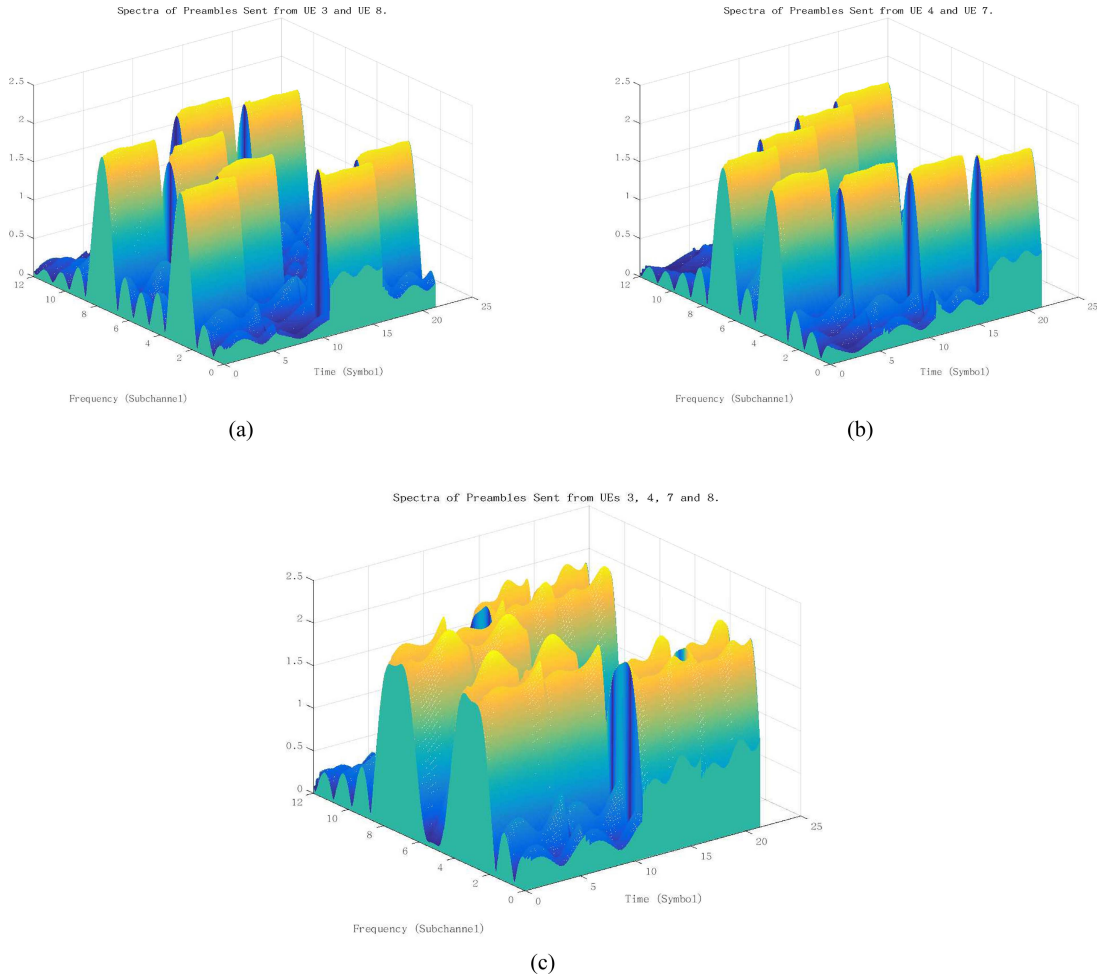
(a)

(b)

(c)

Fig. 2. (a) Spectra of UE 3's and UE 8's first preambles, with no CFOs. (b) Spectra of UE 4's and UE 7's first preambles, with NCFOs of $\epsilon_4 = -0.4$ and $\epsilon_7 = 0.3$. (c) Spectra of UEs 3, 4, 7, and 8.
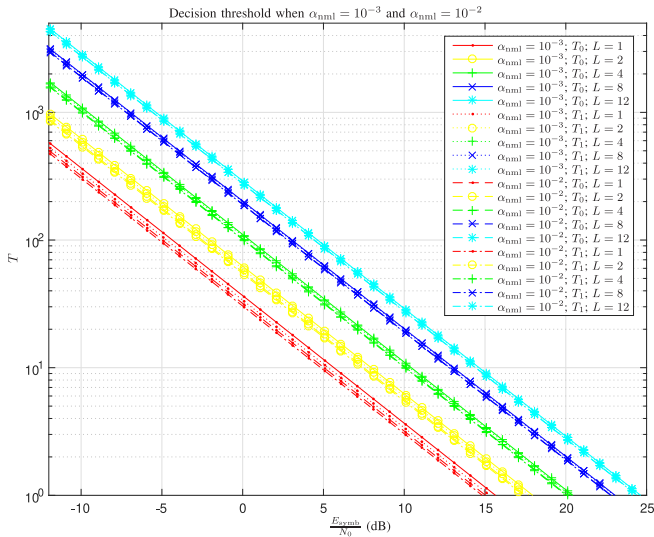

Fig. 3. Decision thresholds evaluated via iterative search and the CLT approximation when $\alpha_{nml} = 10^{-3}$ and 10^{-2}. T_0 is the value determined via the iterative search method, while T_1 is the value calculated via the CLT approximation.

be conducted either by performing zero padding in the TD downsampled stream and then applying the DFT or by using

a bank of TDMFs. Here, $M_{up} = 16$ is chosen unless otherwise mentioned. Demodulation based on a bank of TDMFs eliminates the requirement that the differences in the ToAs all be less than the CP length, which is a presumption of DFT-based demodulation [4], [8], [9]. Thus, the conversion of DFT-based demodulation into TDMF-bank-based demodulation can be used to address the problem of differences of delays investigated in the previous studies [16], [17], [18]. However, solving the problem of large differences of delays is beyond the scope of this article. This article instead focuses on solving the problems presented by multiple nonnegligible CFOs.

For illustration, the spectra of the first preambles of UEs 3, 4, 7, and 8 received at the BS are depicted in Fig. 2. Fig. 2(a) shows the spectra of the first preambles sent from UE 3 and UE 8, with no CFOs. Fig. 2(b) shows the spectra of the first preambles sent from UE 4 and UE 7, with NCFOs of $\epsilon_4 = -0.4$ and $\epsilon_7 = 0.3$, respectively. Fig. 2(c) shows the spectra of the first preambles sent from UEs 3, 4, 7, and 8. Each UE has its own local oscillator and therefore incurs an individual NCFO. The signal powers from UEs 4 and 7 leak into neighboring subchannels because of the nonnegligible CFOs of these UEs. Therefore, the miss probabilities
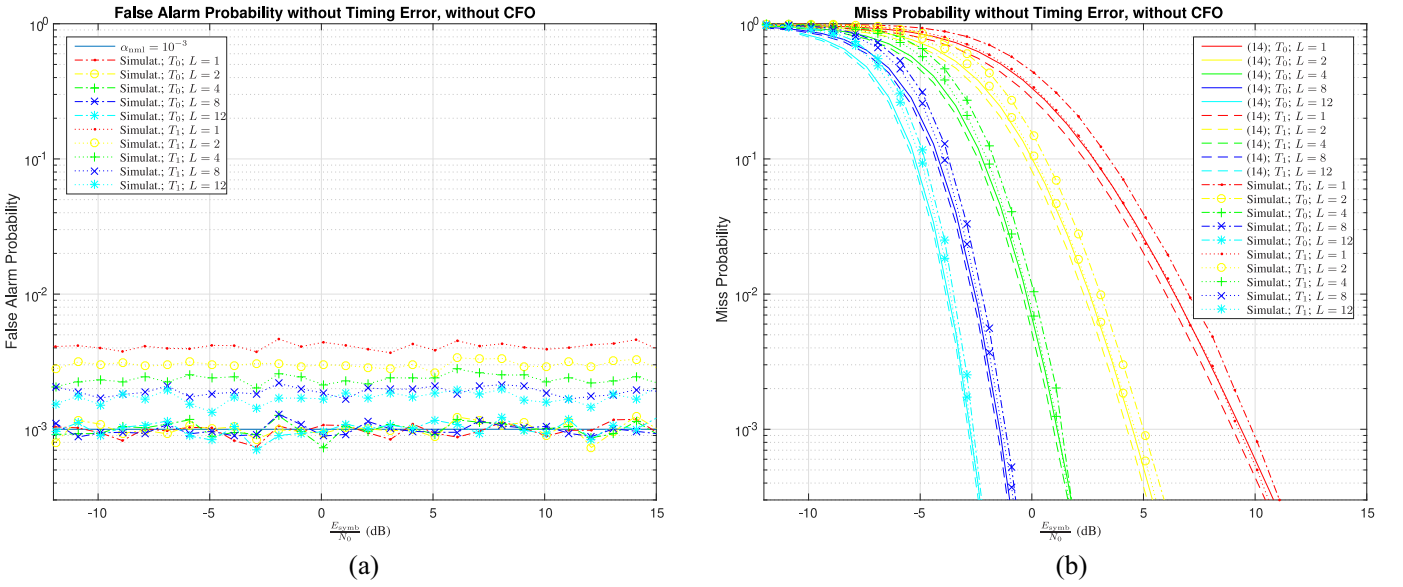
Fig. 4. (a) False alarm probability and (b) miss probability when no TEs and no CFOs are present. T_0 is the value determined via the iterative search method, while T_1 is the value calculated via the CLT approximation.
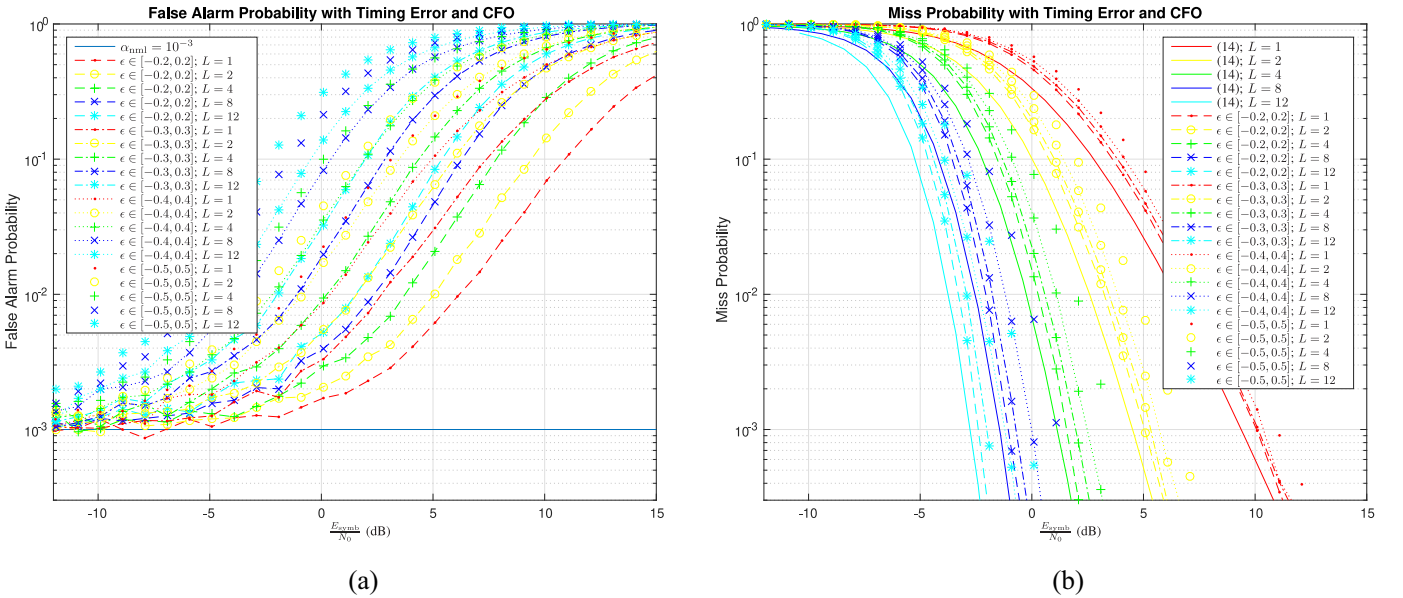

Fig. 5. (a) False alarm probability and (b) miss probability when TEs and CFOs are both present.

for the detection of UE 4 and UE 7 increase. As seen from Fig. 2(c), the spectra of the preambles sent from UEs 3 and 4 overlap with each other, and the spectra of the preambles sent from UEs 7 and 8 also overlap with each other. The subchannels reserved for UEs 5 and 6 should be empty; however, they are instead partially occupied by the spectral sidelobes of UEs 3 and 4, respectively. These spectral sidelobes are undoubtedly ICI, increasing the false alarm probabilities for UE 5 and UE 6.

Although (9) is an exact expression with no nonelementary functions, the relation between the decision threshold T and the NFAP α_{nml} is implicit; in other words, T cannot be expressed as an explicit function of α_{nml} consisting only of elementary functions by solving (9). Therefore, the decision threshold can only be determined via an iterative search method. The search range is set to extend from $\mathsf{E}\{X_{u,L}|H_0\} =$

$40L\sigma_N^2$ to $\mathsf{E}\{X_{u,L}|H_1\}$. The step size Δ_T is chosen to be $1/1024$ of the standard deviation of the RV $X_{u,L}|H_0$, i.e., $\Delta_T = \sqrt{80L\sigma_N^4}\big/1024$. As an alternative to the aforementioned iterative search method, the RV $X_{u,L}|H_0$ can be approximated as a Gaussian RV with mean $40L\sigma_N^2$ and variance $80L\sigma_N^4$ in accordance with the central limit theorem (CLT) [24, p. 278]. Accordingly, (9) can be rewritten as follows:

$$\alpha_{\mathrm{nml}} = \mathsf{Q}\left(\frac{T - 40L\sigma_N^2}{\sqrt{80L\sigma_N^4}}\right) \tag{22}$$

where $\mathsf{Q}(x) = (1/\sqrt{2\pi})\int_x^\infty \exp(-y^2/2)dy$ represents the Gaussian Q-function [21, eq. (2.3-10), p. 41]. Thus, the
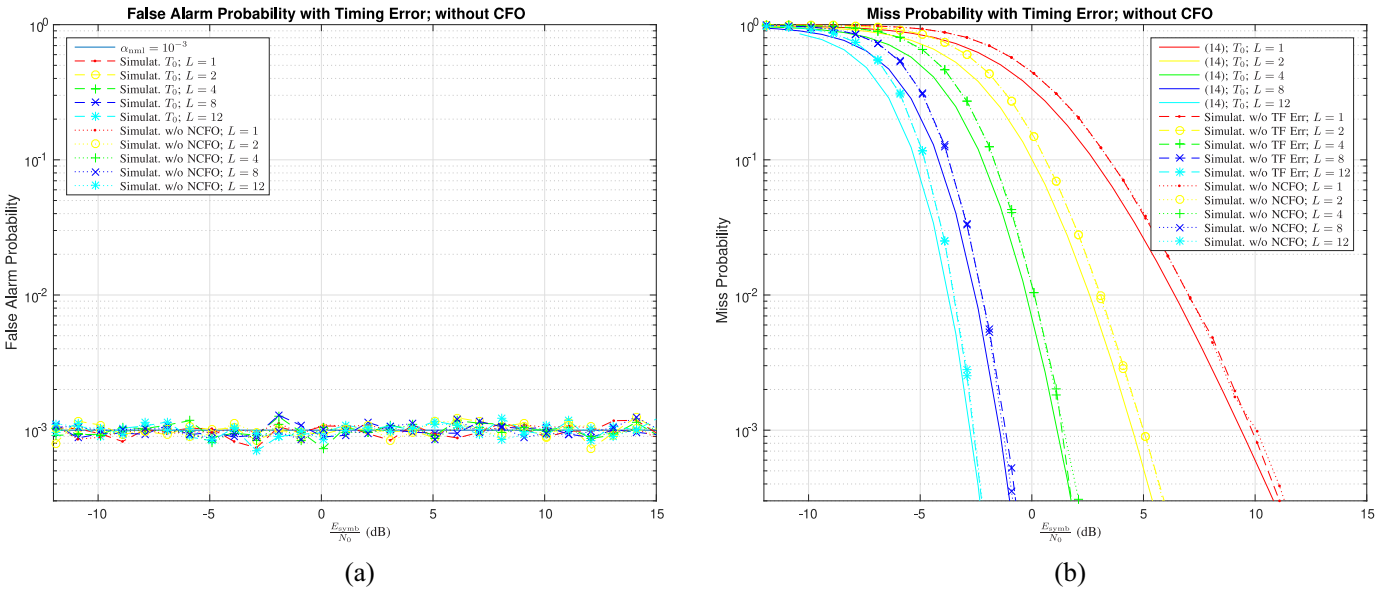
Fig. 6. (a) False alarm probability and (b) miss probability when TEs are present with no CFOs. "w/o NCFO" means "with a TE but no NCFO." "w/o TF Err" means "without TEs or NCFOs."

decision threshold can be approximately calculated as follows:

$$T = \left(\sqrt{80L}\mathsf{Q}^{-1}(\alpha_{\mathrm{nml}}) + 40L\right)\sigma_N^2 \tag{23}$$

where $\mathsf{Q}^{-1}(\cdot)$ represents the inverse of the Gaussian Q-function. The results of both of the above-mentioned threshold determination methods can be precalculated and prestored offline without introducing real-time computational complexity.

Fig. 3 shows the decision thresholds evaluated via the iterative search method and via the CLT approximation when $\alpha_{\mathrm{nml}} = 10^{-3}$ and 10^{-2}. T_0 denotes the value determined via the iterative search method, whereas T_1 denotes the value calculated via the CLT approximation as written in (23). The following three observations are found. First, the thresholds increase as the number of NPRACH preambles, L, increases. Second, T_1 is only slightly lower than T_0. When $L \geq 2$ (i.e., the yellow curves for $L = 2$, the green curves for $L = 4$, the blue curves for $L = 8$, and the cyan curves for $L = 12$), T_0 and T_1 nearly align with each other; thus, the CLT approximation provides high accuracy as L increases. Third, the false alarm probability is very sensitive to the determination of the decision threshold. Even a very slight decrease in the threshold can cause the false alarm probability to increase by one decade.

Fig. 4(a) and (b) shows the false alarm and miss probabilities, respectively, when no NCFOs and no TEs are present. The following five observations are found. First, as seen from Fig. 4(a), the simulation results for the false alarm probability are close to the NFAP, $\alpha_{\mathrm{nml}} = 10^{-3}$, only when T_0 is used. With T_1, the false alarm probability is higher than $\alpha_{\mathrm{nml}} = 10^{-3}$. This is reasonable because T_1 is slightly lower than T_0, as shown in Fig. 3. Second, as seen from Fig. 4(b), the analytical results for the miss probability obtained using either T_0 or T_1 are close to each other, especially when $L \geq 2$. Third, the simulation results for the miss probability are close to the analytical results obtained using (14), especially when $L \geq 4$.

Fourth, because T_1 is slightly lower than T_0, the miss probabilities obtained using T_1 are lower than those obtained using T_0. Fifth, for a target miss probability of 10^{-3}, approximate SNR requirements can be obtained from Fig. 4(b), as follows: $E_{\mathrm{symb}}/N_0 \geq 4$ dB for $L = 2$; $E_{\mathrm{symb}}/N_0 \geq 1$ dB for $L = 4$; $E_{\mathrm{symb}}/N_0 \geq -2$ dB for $L = 8$; and $E_{\mathrm{symb}}/N_0 \geq -3$ dB for $L = 12$. For a target miss probability of 10^{-2}, the approximate SNR requirements obtained from Fig. 4(b) are as follows: $E_{\mathrm{symb}}/N_0 \geq 3$ dB for $L = 2$; $E_{\mathrm{symb}}/N_0 \geq 0$ dB for $L = 4$; $E_{\mathrm{symb}}/N_0 \geq -3$ dB for $L = 8$; and $E_{\mathrm{symb}}/N_0 \geq -4$ dB for $L = 12$. To reduce the miss probability by one decade, the SNR needs to be increased by approximately 1 dB when the decision latency L remains unchanged.

Fig. 5(a) and (b) shows the false alarm and miss probabilities, respectively, when NCFOs and TEs are both present. The NCFOs are assumed to be uniformly distributed in $[-0.2, 0.2]$, $[-0.3, 0.3]$, $[-0.4, 0.4]$, or $[-0.5, 0.5]$, and the TEs are assumed to be uniformly distributed from 0 to one CP length. The following five observations are found. First, as seen from Fig. 5(a), the false alarm probability exceeds the NFAP of $\alpha_{\mathrm{nml}} = 10^{-3}$, especially when detection is performed in the interference-dominant regime (i.e., $E_{\mathrm{symb}}/N_0 \geq 0$ dB). Second, the false alarm probability increases as the SNR (or E_{symb}/N_0) increases because of the interference-dominant regime. Third, the false alarm probability increases as L increases due to the interference-dominant regime. The summation (or integrate-and-dump filter) functioning as an LPF rejects out-band noise. A larger value of L can only reduce the noise variance, thereby causing the ICI to become dominant and thus increasing the false alarm probability. Fourth, as seen from Fig. 5(b), the miss probability increases because the spectral sidelobes of the NPRACHs unavoidably leak into adjacent subchannels due to the nonnegligible CFOs. Fifth, both the false alarm and miss probabilities increase as the NCFOs increase.
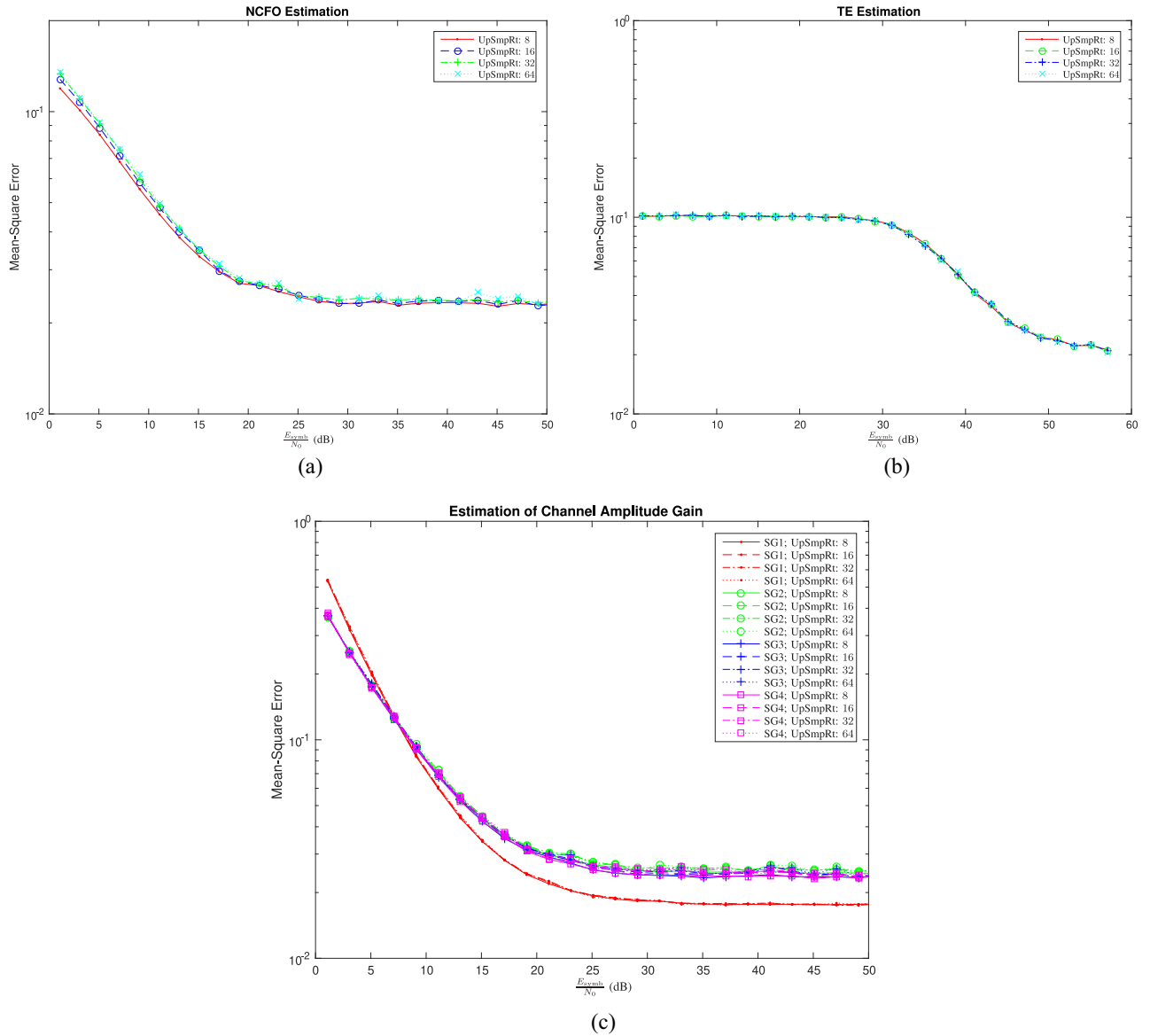
Fig. 7. Mean-square estimation errors for the (a) NCFO, (b) TE, and (c) magnitude of channel gain. "UpSmpRt" stands for the upsampling rate in the frequency domain.

Fig. 6(a) and (b) shows the simulation results for the false alarm and miss probabilities, respectively, when TEs are present with no NCFOs. The false alarm and miss probabilities shown in Fig. 6(a) and (b) are close to those shown in Fig. 4(a) and (b), respectively. As seen by comparing Figs. 4–6, the observed increases in the false alarm and miss probabilities mainly result from the presence of multiple NCFOs, not from TEs.

Fig. 7(a) and (b) shows the mean-square errors of the JMLE of the NCFO and TE, respectively, as expressed in (18). As seen from Fig. 7(a), a mean-square estimation error of 10^{-2} can be achieved for the estimated NCFO. The TE estimation errors are normalized with respect to the CP length. As seen from Fig. 7(b), an error on the level of approximately 10% to 30% of the CP length is incurred in TE estimation. A lower error cannot be achieved when estimating the TE because the ambiguity function expressed in (20) and shown in Fig. 1 has a flat top in the Δl_u direction. TE estimation can be conducted

only by determining the boundaries of an SG instead of those of a symbol because an SG is composed of five identical symbols and one CP. A continuous wave has been proven to be an effective training preamble for CFO estimation, but it is not effective for TE estimation because an NPRACH symbol, which is a complex sinusoidal waveform, has a narrow mean-square bandwidth and a long mean-square symbol duration. The mean-square errors of the JMLE of the NCFO and TE are inversely proportional to the mean-square symbol duration and the mean-square bandwidth, respectively, as shown in [6, eq. (12)]. After JMLE of the NCFO and TE has been performed, the TDMF output can be regarded as the ML channel estimate, as follows:

$$\hat{w}_{u,v} = \frac{1}{N} \sum_{k=0}^{N-1} r[k] \exp\left(-j\left(2\pi\left(v + \frac{\hat{\epsilon}_u}{N}\right)\left(k - \hat{l}_u\right)\right)\right). \quad (24)$$
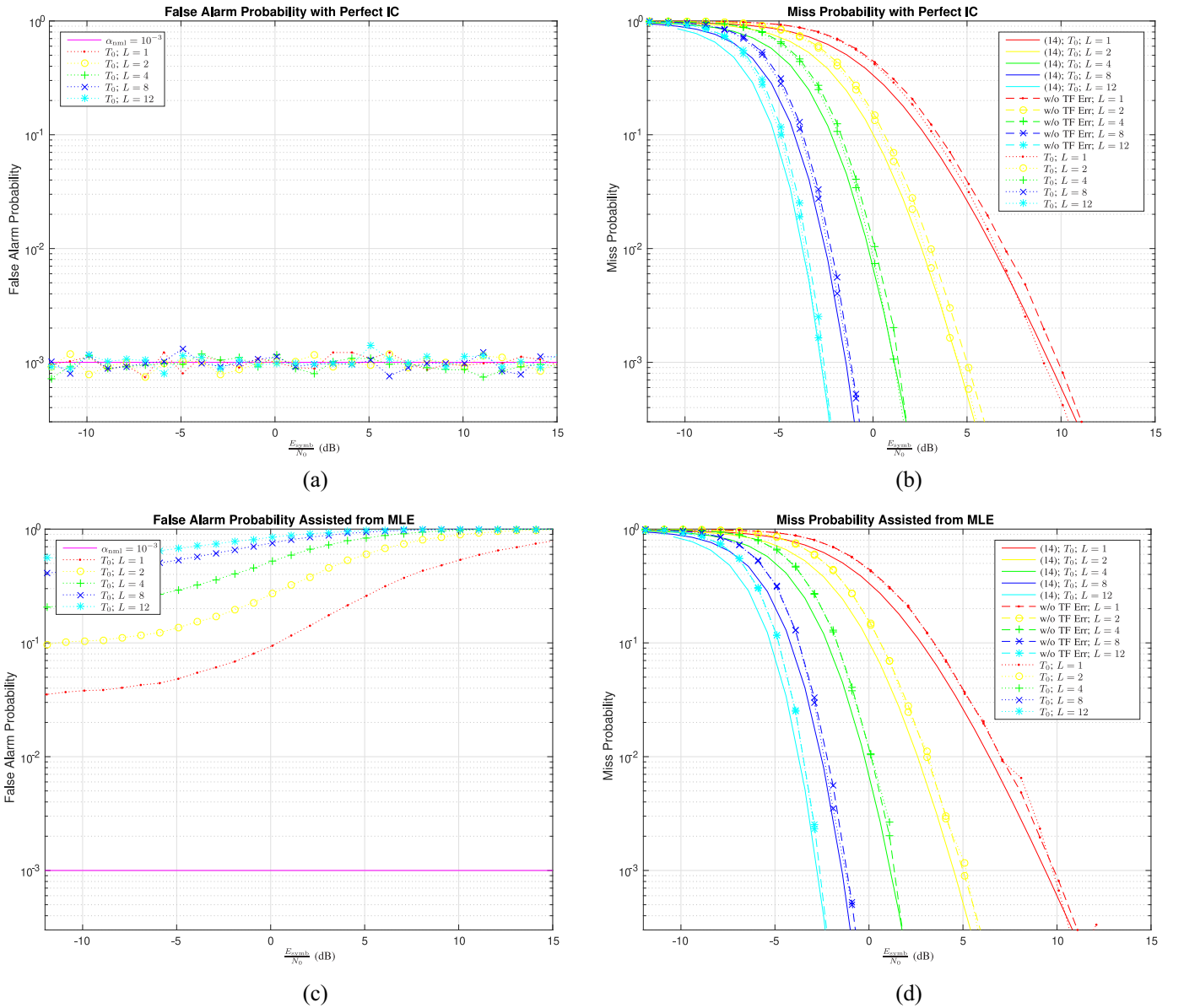
Fig. 8. (a) False alarm probability and (b) miss probability obtained using the IRnC method with perfect estimates. (c) False alarm probability and (d) miss probability obtained using the IRnC method with ML estimates. "w/o TF Err" means "without TEs or NCFOs."

Unfortunately, the initial phase error $\phi_{u,0}$ in (18) is an unknown RV and changes with every symbol, and a nonzero $\Delta\epsilon_u$ and a nonzero Δl_u cause ϕ_M in (18) to be undetermined. Therefore, the complex-valued channel gain estimator in (24) cannot be applied due to the aforementioned phase rotations. Fig. 7(c) shows the mean-square estimation errors for the magnitude of the channel gain.

An IRnC method similar to that presented in a previous study [20] is used for forward error reduction. Fig. 8(a) and (b) shows the false alarm and miss probabilities, respectively, when perfect estimates of the NCFOs, TEs, and channel gains are used to regenerate and cancel the ICI at the receiving end. The false alarm and miss probabilities decrease and approach those obtained with no NCFOs. Fig. 8(c) and (d) shows the false alarm and miss probabilities,

respectively, when the JMLE in (18) and the channel estimator in (24) are used instead to regenerate and cancel the ICI at the receiving end. As seen from Fig. 8(d), the miss probabilities again decrease close to those obtained with no NCFOs. This result occurs because the NCFO estimates are highly accurate, enabling the TDMFs to be tuned to effectively acquire the corresponding NPRACH signals in the right subchannel bands. However, because the unknown initial phase errors $\phi_{u,0}$ and residual TEs lead to random phase rotations in the channel estimates, the IRnC method cannot perfectly regenerate and cancel the ICI; consequently, the false alarm probability increases, as shown in Fig. 8(c).

Based on the above simulations, it is found that individual CFOs lead to ICI and result in increases in both the false alarm and miss probabilities. Although the IRnC method for
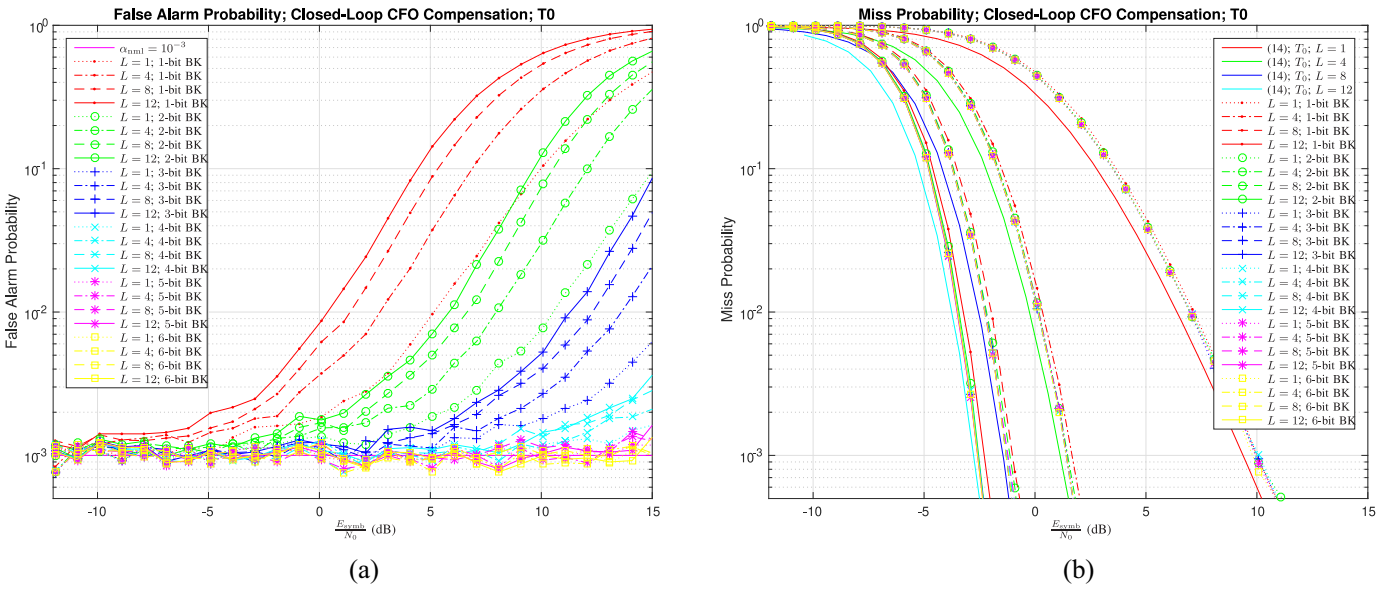
Fig. 9. (a) False alarm probability and (b) miss probability with CLCC using 2- to 6-bit quantized NCFO estimates. "BK" stands for "NCFO estimate sent back to the corresponding UE."

forward error reduction does not require extra radio resources, it can only reduce the miss probability and cannot reduce the false alarm probability. However, if the serving BS sends ML estimates of the NCFOs back to the corresponding UEs via RAR, i.e., Message 2 of the PRACH procedure [18], or via dedicated channels for another RA attempt, then the UEs can compensate for the CFOs prior to sending their NPRACH preambles. For this purpose, the ML NCFO estimates need to be quantized to a few bits to reduce the consumption of radio resources [25]. Several quantization techniques have been thoroughly investigated in a previous study [25]. The uniform quantization in [25, eq. (34)] is used in the following simulations. Fig. 9(a) and (b) shows the false alarm and miss probabilities, respectively, when the ML NCFO estimates are quantized and delivered to the corresponding UEs for CLCC. As seen from Fig. 9(b), the miss probabilities decrease to the level of those obtained with no CFOs. As seen from Fig. 9(a), the false alarm probabilities also decrease due to the decrease in the ICI as the number of quantization bits increases. When the number of quantization bits exceeds 5, the false alarm probabilities decrease to the level of the NFAP, $\alpha_{\text{nml}} = 10^{-3}$.

IV. CONCLUSION

This article has proposed and comprehensively investigated a novel technique to effectively detect superimposed NPRACH preambles, accurately estimate individual CFOs, and ultimately reduce ICI, thereby maintaining low false alarm and miss probabilities. The false alarm and miss probabilities have been derived in the presence of frequency selectivity, time selectivity, and different channel conditions for the NPRACH preambles from different UEs. To reduce the ICI, which mainly results from the different CFOs, a forward error reduction method assisted by IRnC has been proposed and thoroughly studied. The IRnC method has been found to effectively reduce the miss probability. The CLCC

method has been proven to effectively maintain low false alarm and miss probabilities simultaneously by sending quantized NCFO estimates back to the corresponding UEs via RAR messages or other dedicated channels. Computer simulations conducted to confirm the theoretical analyses have shown that the proposed technique achieves low false alarm and miss probabilities.

REFERENCES

[1] M. Kanj, V. Savaux, and M. L. Guen, "A tutorial on NB-IoT physical layer design," *IEEE Commun. Surveys Tuts.*, vol. 22, no. 4, pp. 2408–2446, 4th Quart., 2020.

[2] W. S. Jeon, S. B. Seo, and D. G. Jeong, "Effective frequency hopping pattern for ToA estimation," *IEEE Trans. Veh. Technol.*, vol. 67, no. 10, pp. 10150–10154, Oct. 2018.

[3] R. Harwahyu, R.-G. Cheng, C.-H. Wei, and R. F. Sari, "Optimization of random access channel in NB-IoT," *IEEE Internet Things J.*, vol. 5, no. 1, pp. 391–402, Feb. 2018.

[4] X. Lin, A. Adhikary, and Y.-P. E. Wang, "Random access preamble design and detection for 3GPP narrowband IoT systems," *IEEE Wireless Commun. Lett.*, vol. 5, no. 6, pp. 640–643, Dec. 2016.

[5] N. Levanon and E. Mozeson, *Radar Signals*. Hoboken, NJ, USA: Wiley, 2004.

[6] J.-C. Lin, "Initial synchronization assisted by inherent diversity over time-varying frequency-selective fading channels," *IEEE Trans. Wireless Commun.*, vol. 13, no. 5, pp. 2518–2529, May 2014.

[7] J.-C. Lin, Y.-T. Sun, and H. V. Poor, "Initial synchronization exploiting inherent diversity for LTE sector search process," *IEEE Trans. Wireless Commun.*, vol. 15, no. 2, pp. 1114–1128, Feb. 2016.

[8] S. Cho, H. Kim, and G. Jo, "Determination of optimum threshold values for NPRACH preamble detection in NB-IoT system," in *Proc. 10th Int. Conf. Ubiquitous Future Netw. (ICUFN)*, 2018, pp. 616–618.

[9] J.-K. Hwang, C.-F. Li, and C. Ma, "Efficient detection and synchronization of superimposed NB-IoT NPRACH preambles," *IEEE Internet Things J.*, vol. 6, no. 1, pp. 1173–1182, Feb. 2019.

[10] Q. Wu, P. Wu, W. Wen, T. Yang, and M. Xia, "An efficient NPRACH receiver design for NB-IoT systems," *IEEE Internet Things J.*, vol. 7, no. 10, pp. 10418–10426, Oct. 2020.

[11] G. Giunta, A. Neri, and L. Vandendorpe, "Initial code synchronization of W-CDMA mobile systems exploiting local phase coherence and Pisarenko estimation," *IEEE Trans. Commun.*, vol. 53, no. 1, pp. 48–52, Jan. 2005.

[12] F. Aoudia, J. Hoydis, S. Cammerer, M. van Keirsbilck, and A. Keller, "Deep learning-based synchronization for uplink NB-IoT," in *Proc. IEEE Global Commun. Conf.*, 2022, pp. 1478–1483.

[13] Y. R. Kumar and N. M. Balasubramanya, "Deep learning based random access preamble detection for 3GPP NB-IoT systems," in *Proc. IEEE Wireless Commun. Netw. Conf. (WCNC)*, 2022, pp. 1689–1694.

[14] H. Chougrani, S. Kisseleff, and S. Chatzinotas, "Efficient preamble detection and time-of-arrival estimation for single-tone frequency hopping random access in NB-IoT," *IEEE Internet Things J.*, vol. 8, no. 9, pp. 7437–7449, May 2021.

[15] J.-C. Lin, "Differentially coherent PN code acquisition with full-period correlation in chip-synchronous DS/SS receivers," *IEEE Trans. Commun.*, vol. 50, no. 5, pp. 698–702, May 2002.

[16] H. Chougrani, S. Kisseleff, W. A. Martins, and S. Chatzinotas, "NB-IoT random access for nonterrestrial networks: Preamble detection and uplink synchronization," *IEEE Internet Things J.*, vol. 9, no. 16, pp. 14913–14927, Aug. 2022.

[17] X. Liu and D. Gokhale, "GNSS-independent acquisition for NTN NB-IoT," in *Proc. 39th Int. Commun. Satell. Syst. Conf. (ICSSC)*, 2022, pp. 164–168.

[18] O. Kodheli et al., "Random access procedure over non-terrestrial networks: From theory to practice," *IEEE Access*, vol. 9, pp. 109130–109143, 2021.

[19] A. D. Whalen, *Detection of Signals in Noise*. San Diego, CA, USA: Academic, 1971.

[20] J.-C. Lin, "A modified PN code tracking loop for direct-sequence spread-spectrum communication over arbitrarily correlated multipath fading channels," *IEEE J. Sel. Areas Commun.*, vol. 19, no. 12, pp. 2381–2395, Dec. 2001.

[21] J. G. Proakis and M. Salehi, *Digital Communications*, 5th ed. Boston, MA, USA: McGraw-Hill, 2008.

[22] R. H. Clarke, "A statistical theory of mobile radio reception," *Bell Syst. Tech. J.*, vol. 47, no. 6, pp. 957–1000, Jul./Aug. 1968.

[23] W. C. Jakes, *Microwave Mobile Communications*. New York, NY, USA: Wiley, 1974.

[24] A. Papoulis and S. U. Pillai, *Probability, Random Variables and Stochastic Processes*, 4th ed. Boston, MA, USA: McGraw-Hill, 2002.

[25] J.-C. Lin, H.-K. Chang, M.-L. Ku, and H. V. Poor, "Impact of imperfect source-to-relay CSI in amplify-and-forward relay networks," *IEEE Trans. Veh. Technol.*, vol. 66, no. 6, pp. 5056–5069, Jun. 2017.

Jia-Chin Lin (Senior Member, IEEE) received the B.S. and M.S. degrees from the Department of Electronics Engineering, National Chiao Tung University (NCTU), Hsinchu, Taiwan, in 1994 and 1995, respectively, and the Ph.D. degree from National Taiwan University, Taipei, Taiwan, in 1998.

He was in the Obligatory Military Service from July 1998 to March 2000 and then joined the Microelectronics and Information Systems Research Center, NCTU as a Research Assistant Professor. In February 2001, he joined the Department of Electrical Engineering, National Chi Nan University, Nantou, Taiwan, as an Assistant Professor. In August 2004, he was promoted to serve as an Associate Professor. In August 2006, he joined the faculty with the Department of Communication Engineering, National Central University, Taoyuan City, Taiwan, as an Associate Professor. In August 2008, he was promoted to serve as a Full Professor. In January 2011, he became a Distinguished Professor. He has also held visiting appointments at several universities, including with Stanford University, Stanford, CA, USA, and Princeton University, Princeton, NJ, USA.

Dr. Lin was receipt of several awards in recognition of his work includes the Dr. Wu Da-You Research Award from the National Science Council, Executive Yuan, the 2003 Award for Outstanding Faculty from the Ministry of Education, the Young Scientist Award issued by URSI, the Outstanding Researcher Award from the IEEE ComSoc APB, the Investigative Research Award (for visiting scholarship) from the Pan Wen Yuan Foundation, the Taiwan Merit Scholarships Program from Executive Yuan, and the 2009 Ten Outstanding Young Persons Award of Taiwan. He has been serving as an (Associate) Editor for IEEE TRANSACTIONS ON VEHICULAR TECHNOLOGY from 2008. He has been serving as a Technical Associate Editor for *IEEE Communications Magazine* from 2013. He had served as an Associate Editor for IEEE SIGNAL PROCESSING LETTERS from 2011 to 2012. He served as a Guest Editor for IEEE JOURNAL ON SELECTED AREAS IN COMMUNICATIONS (Special Issue on Emerging Technologies in Communications: Vehicular Networks and Telematics Applications). He served as a Guest Editor for *IEEE ITS Magazine* and *IET Intelligent Transport Systems*. He served as the Lead Guest Editor for IEEE TRANSACTIONS ON VEHICULAR TECHNOLOGY (SPECIAL ISSUE ON TELEMATICS ADVANCES FOR VEHICULAR COMMUNICATION NETWORKS) in 2011. He is a Fellow of the IET.